RSC Advances

PAPER

View Article Online
View Journal | View Issue

Check for updates

Cite this: *RSC Adv.*, 2024, **14**, 19147

Flash precipitation of random copolymers in a micro-mixer for controlling the size and surface charge of nanoparticles†

Jeong-Un Joo,‡[a] Chae-Hyeon Park,‡[a] Jianwen Yang,[a] Yoonseok Ko,[b] Sang Soo Jee,[b] Hyungju Ahn[c] and Dong-Pyo Kim*[a]

Received 24th February 2024
Accepted 19th May 2024

DOI: 10.1039/d4ra01433b

rsc.li/rsc-advances

Precisely controlling the size and surface chemistry of polymeric nanoparticles (P-NPs) is critical for their versatile engineering and biomedical applications. In this work, various NPs of amphipathic random copolymers were comparatively produced by the flash nanoprecipitation (FNP) method using a tube-in-tube type of micro-mixer up to 330 mg min^{-1} in production scale in a kinetically controlled manner. The NPs obtained from poly(styrene-*co*-maleic acid), poly(styrene-*co*-allyl alcohol), and poly(methyl methacrylate-*co*-methacrylic acid) were concurrently controlled in the range 51–819 nm in size with narrow polydispersity index (<0.1) and −44 to −16 mV in zeta potential, by depending not only on the polymeric chemistry and the concentration but also the mixing behavior of good solvents (THF, alcohols) and anti-solvent (water) under three flow regimes (laminar, vortex and turbulence, turbulent jet). Moreover, the P(St-MA) derived NPs under turbulent jet flow conditions were post-treated in the initial solution mixture for up to 16 h, resulting in lowering of the zeta potential to −52 mV from the initial −27 mV and decreasing size to 46 nm from 50 nm by further migration of hydrophilic segments with –COOH groups on the outer surface, and the removal of THF trapped in the hydrophobic core.

1 Introduction

Polymeric nanoparticles (P-NPs) have been used for a wide range of applications such as drug delivery, vaccines, and bioimaging.[1–3] Amphipathic block copolymers have been widely explored for P-NPs precipitation, due to their well-defined structure. Conversely, amphipathic random copolymers lack a specific pattern in the arrangement of hydrophilic and hydrophobic segments which are distributed randomly along the polymer chain.[4–6] The utilization of random copolymers with structural diversity and ease of synthesis offers certain advantages for large-scale production over high-cost block copolymers. However, due to the lack of a well-defined and organized structure, random copolymers may have weaker intermolecular connections, and P-NPs are more likely to deteriorate or disintegrate. The disordered arrangement of segments and variable degradation severely limits their application in certain P-NPs syntheses.[7,8] Over the years, a plethora of studies have been dedicated to exploring the self-assembly behaviour of random copolymers, leading to the creation of P-NPs with a wide range of morphologies.[9–14] Initially, in 2005 Eisenberg's group successfully utilized random copolymer poly(styrene-*co*-maleic acid) P(St-MA) to self-assemble into bowl-like P-NPs. In 2011, Zhu and Liu conducted the self-assembly and morphology control of L-glutamic acid-based amphipathic random copolymers, leading to the formation of (micro)vesicles, spheres, and honeycomb membrane P-NPs. Further experimental findings have interpreted that the polymer composition, the degree of polymerization, and the nature of hydrophobic segments and spacers between polymer backbones play a crucial role in shaping the interactions within the side chains of random polymers. However, there are a few concerns about the influence of fluid dynamics impact on random copolymer nanoprecipitation in microfluidic mixers. The Flash nanoprecipitation (FNP) process accomplished within several milliseconds is a highly simple and rapid flow-based synthesis method of NPs in a micro-mixer. This FNP method addresses the inherent issues of bulk synthesis, where the low mixing efficiency generally cased non-uniformity in size and the distribution as well as low reproducibility.[15–17]

In this work, we accessed the turbulent jet regime, inaccessible by conventional micro-mixers, *via* FNP, thereby achieving high mixing efficiency. Leveraging these advantages, we synthesized highly uniform nanoparticles using amphiphatic

[a]*Center of Intelligent Microprocess of Pharmaceutical Synthesis, Department of Chemical Engineering, Pohang University of Science and Technology (POSTECH), Pohang, 37673, Korea. E-mail: dpkim@postech.ac.kr*

[b]*Samsung Advanced Institute of Technology (SAIT), Suwon 16678, Republic of Korea*

[c]*9A U-SAXS Beamline (PLS-II), Pohang Accelerator Laboratory (PAL), POSTECH, Republic of Korea*

† Electronic supplementary information (ESI) available: Full experimental details and characterisation. See DOI: https://doi.org/10.1039/d4ra01433b

‡ These authors equally contributed to this work.

Open Access Article. Published on 14 June 2024. Downloaded on 12/27/2025 2:59:57 PM. This article is licensed under a Creative Commons Attribution-NonCommercial 3.0 Unported Licence.

Open Access Article. Published on 14 June 2024. Downloaded on 12/27/2025 2:59:57 PM. This article is licensed under a Creative Commons Attribution-NonCommercial 3.0 Unported Licence.

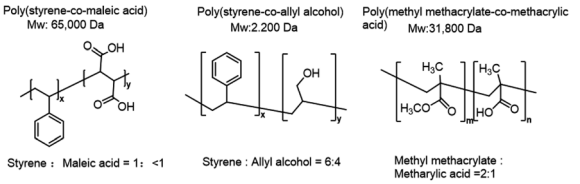

Fig. 1 Chemical structure and molecular weight of three random copolymers: P(St-MA), P(St-AA), P(MMA-MAA).

random copolymers with inconsistent molecular structures (Fig. 1). Initially, the fluid behaviors in a tube-in-tube type of micro-mixer were visualized to clearly distinguish three flow regimes (laminar, vortex and turbulence (V&T), turbulent jet) with different mixing efficiencies under Reynolds numbers of >500 and a flow rate ratio of 1 : 9.6. Based on Hansen solubility parameters, THF as a good solvent with alcoholic co-solvents, water as an anti-solvent were commonly selected for the FNP of three random copolymers, P(St-MA), poly(styrene-*co*-allyl alcohol) (P(St-AA)), and poly(methyl methacrylate-*co*-methacrylic acid) (P(MMA-MAA)) to investigate the effect of mixing conditions, concentrations of polymers, on size/distribution and zeta potential of obtained P-NPs. Moreover, the obtained P-NPs were post-treated in the initial solution mixture up to 16 h, resulting in lowering zeta potential and decreasing size by further structural rearrangement into a self-assembled. In particular, it is anticipated that carboxyl, hydroxyl groups on the surface of P-NPs facilitate further functionalization for various applications.

2 Experimental

2.1. Assembly of modular micro-mixer

Scheme 1A shows the streamlines of a 3D flow-focusing device for two different distances between the inlet channel and the outlet channel: a device of tube-in-tube type that has two different distances between the inlet channel and the outlet channel: 1/100″ and 1/33″ as reported by H. Han *et al.* (2021).[18] Three FEP tubings (OD = 1/8″ and ID = 1/16″, IDEX Health & Sciences) were connected to ETFE cross (OD = 1/8″, P-635, IDEX Health & Science) using flangeless fitting (XP-345, IDEX Health and Science). At this point, the tubing in the middle becomes the outlet, and the tubing on both sides becomes the inlet of non-solvent. On the opposite side of the outlet, connect the FEP tubing (OD = 1/25″ and ID = 1/50″, IDEX Health & Science) in the form of a tube-in-tube type by penetrating the ETFE cross. NanoTight Tubing Sleeve (F-252X, Health & Science) and Flangeless Fitting were used to fix the FEP Tubing. One FEP tubing in the form of a tube-in-tube type by penetrating the ETFE cross must be kept in the center of the cross-body. Nano tight tubing sleeve and flangeless fitting were used to fix the FEP tubing.

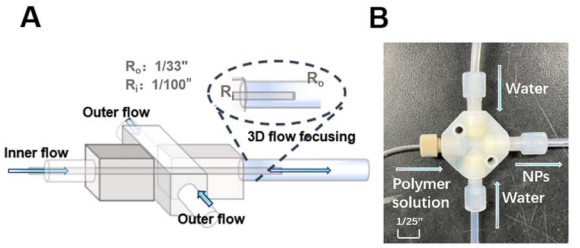

Scheme 1 (A) Schematic diagram of tube-in-tube type of micro-mixer as a FNP generator. (B) Photographs of the assembled FNP.

2.2. Calculation of Hansen solubility parameter (HSP)

HSP has been used as an index to show the affinity between substances, which is a quantitative way to predict whether a substance dissolves in a solvent to form a solution.[19,20] In principle, the HSP of each molecule is defined as the sum of three interaction energies (dispersion force δ_d, dipole intermolecular force δp, and hydrogen bonding δ_H) between molecules. The three parameters are expressed in Hansen space as *a* point of 3D coordinates, so molecules located close together in the Hansen space are more likely to dissolve into each other. To determine if the parameters of the solvent molecule (1) and the polymer (2) are within a close range, the interaction radius (Ra) value of the sphere in Hansen space was calculated according to the following formula (see the details in Section 1.2 of ESI†).

$$R_a = [4(\delta_{d,2} - \delta_{d,1})^2 + (\delta_{p,2} - \delta_{p,1})^2 + (\delta_{h,2} - \delta_{h,1})^2]^{1/2}$$

2.3. Screening of flow regimes in the micro-mixer

By directing the P-NPs precursor through the inner tube and the anti-solvent through the outer tube, we can effectively maintain a fixed ratio of these components. To visually check the flow regimes, red ink (InkTec H8950D) dissolved in THF solvent was injected as the internal streams, and DI water as outer streams with a flow rate ratio of 1 : 9.6 by controlling the flow rate by two syringe pumps (PHD ULTRA, Harvard Apparatus). This ratio plays a crucial role as an essential parameter in determining the size distribution of P-NPs.[21] The flow rate was controlled using syringe pumps to screen the Reynolds number (Re) while fixing the geometry of the turbulent jet mixer and the composition of the solution. Re ($Re = QD/\nu A$, Q = volumetric flow rate, ν = kinematic viscosity, D = diameter, A = cross-sectional area) and the linear velocity ratio ($R = u_i/u_0$, u_i = linear velocity of inner flow, u_0 = linear velocity of outer flow), were calculated to determine flow regimes of laminar, vortex and turbulence (V & T), and turbulent jet. And the flow rate showing the most perfect flow pattern of each flow regime was chosen one by one.

2.4. Flash nanoprecipitation (FNP) in a micro-mixer

Amphipathic random copolymers, poly(styrene-*co*-maleic acid) (P(St-MA), Sigma), poly(styrene-*co*-allyl alcohol) (P(St-AA), Sigma), and poly(methyl methacrylate-*co*-methacrylic acid) (P(MMA-MAA), Evonik) were dissolved in the mixture of THF and EtOH or MeOH as a co-solvent at a desired concentration (0.1–30 mg mL^{-1}) under magnetic stirring for 30 min (Fig. 1). The polymer solutions and deionized water (DI) as an anti-solvent were injected into the inner and outer channels of

© 2024 The Author(s). Published by the Royal Society of Chemistry

Open Access Article. Published on 14 June 2024. Downloaded on 12/27/2025 2:59:57 PM.
This article is licensed under a Creative Commons Attribution-NonCommercial 3.0 Unported Licence.

micro-mixer, respectively. All experiments were carried out at 25 °C. For comparison, the bulk synthesis was implemented by adding 100 mL of P(St-MA) solution dropwise and mixed with 960 mL of DI water for 2 h.

2.5. Post-treatment of the obtained nanoparticles

The post-treatment was carried out in the initial mixed solution by transferring the as-synthesized P-NPs suspension in 100 mL glass vial into 15 mL glass vial.[22,23] And the samples were placed at room temperature for 16 h to allow gradual evaporation of organic solvents, leading to further self-assembly in the particle.

2.6. Characterization

The size distributions and surface charge of the P-NPs were measured using dynamic light scattering (DLS) with a Zetasizer Nano ZS (Malvern Instruments Ltd). The morphologies of the P-NP were investigated by small-angle X-ray scattering (SAXS), Synchrotron experiments were performed at 9A beamlines in the Pohang Accelerator Laboratory.

3 Results and discussion

3.1. Solvent selection by Hansen solubility parameter (HSP)

HSP indicates the degree of polymer solubility in the solvent by calculating the numerical values from the reported process (See the details in ESI† section 1.2, Table S2, S3, S4†). Hence, the R_a was obtained to determine the degree of solubility of polymer in the solvent using the HSPs.[20] With ease, the smaller R_a values, the greater solubility. And the solvent with the lowest R_a was selected as a good solvent for polymers, while the solvent with the largest R_a is chosen as an anti-solvent. The substantial variation in R_a between solvent and anti-solvent stands out as the primary driving force to produce P-NPs in the FNP. Table 1 summarizes the R_a of polymers in solvents in this study. For the selected three amphipathic random polymers, it becomes evident that the largest discrepancy in solubility parameters exists between THF and water. Based on these, it is commonly confirmed that THF is the good solvent and water is the anti-solvent for P(St-AA), P(St-MA), and P(MMA-MAA) to possibly render finely dispersed P-NPs.

3.2. Analysis of flow behavior in a micro-mixer

The 3D flow-focusing mixer provides a valuable tool for FNP to offer precise control, enhance mass transfer, reduce agglomeration, and improve reaction kinetics.[18] In general, the micro-mixer exhibits various flow regimes of fluid by experimentally adjusting the inner and outer flow rates, as defined by Reynolds number (Re) and linear velocity ratio (R) conditions.[19] The Re as the ratio of inertial force to viscous force is commonly used to identify flow patterns, while the R of the inner flow of THF mixed with ink and the outer flow of DI water is also another important factor in determining the flow regimes (Fig. 2A). Through an open computer vision (CV) program, the different mixing flow patterns depending on the conditions were calculated by converting the red ink images into quantitative Re values, as shown in Table 2 (Fig. S1,† and the details in ESI† section 1.1).

The same approach was used to screen three flow regimes: laminar, vortex and turbulence (V&T), and turbulent jet. It was found that, regardless of the R, at low Re like 678, both the inner and outer flows remain distinct without significant mixing and show a laminar flow regime that maintains a core–shell type of straight line by dividing the layers. In the region where Re is 1865, a turbulent jet regime is shown where the inner flow spreads widely in the form of a spray from the end of the inner tubing. When Re is 1017 which is between the laminar and turbulent jet, it shows a V&T regime where the inner flow is slightly linear at first but fluctuates due to the influence of the outer flow (Fig. 2B and C). As expected, rapid mixing occurred in the turbulent jet and slow mixing exhibited in the laminar. At the entry point with a retention time of 80–82 ms, the turbulent

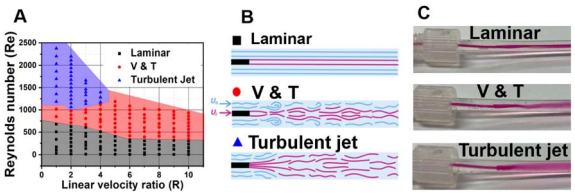

Fig. 2 (A) Phase diagram of flow regime in terms of R and Re for THF. (B) Schematic illustrations of fluid flow at laminar, vortex and turbulence, and turbulent jet regime. (C) Top view of fluid flow at laminar (R = 1 and Re = 678), vortex and turbulence (V & T, R = 1 and Re = 1017), and turbulent jet (R = 1 and Re = 1865) regimes.

Table 2 Flow conditions of three flow regimes in a micro-mixer at different Re values

Flow regimes	Laminar (Re = 678)	V & T (Re = 1017)	Turbulent jet (Re = 1865)
Inner flow rate (ml min^{-1})	4	6	11
Outer flow rate (ml min^{-1})	38	57	105

Table 1 Calculated radius (R_a) values between polymers and solvents

	Solvent							
Polymer	THF	Acetone	Chloroform	Toluene	DMF	EtOH	MeOH	Water
P(St-AA)	0.8	6.0	4.0	8.0	8.7	11.6	15.8	35.5
P(St-MA)	2.0	4.1	4.7	7.8	8.3	13.1	16.9	36.9
P(MMA-MAA)	4.2	5.2	7.7	11.1	8.7	9.7	13.5	33.6

Open Access Article. Published on 14 June 2024. Downloaded on 12/27/2025 2:59:57 PM. This article is licensed under a Creative Commons Attribution-NonCommercial 3.0 Unported Licence.

jet showed a mixing efficiency of 92%, while the V&T showed a mixing efficiency of 61%. In the laminar flow regime, mixing efficiency has been difficult to quantify because diffusion-based laminar flow with low Re results in very low mixing efficiency (Fig. S1 and Table S1†).

3.3. Flash nanoprecipitation of random copolymers under three flow regimes

It is well known that microfluidic approaches with a short diffusive length at the microscale level have provided better control with excellent reproducibility over NP size and PDI by simply manipulating the flow rate of the polymer solution and anti-solvent[24]. In the FNP, the rapid interdiffusion mixing of the solvent and anti-solvent causes the local composition of the suspending solution to swiftly pass through the critical precipitation condition. It was well documented that the precipitation process involves two phases along with the La Mer mechanism:[25] nucleation and growth. Nucleation occurs when concentration surpasses supersaturation, growing to larger particles in low supersaturation of slow mixing, but to smaller and uniform ones in high supersaturation of fast mixing.

In this work, we employed three types of amphipathic random copolymers: P(St-AA) at a concentration of 3 mg ml^{-1}, P(St-MA) at 7 mg ml^{-1}, and P(MMA-MAA) at 7 mg ml^{-1}. These P-NPs were produced to thoroughly investigate the effect of flow regimes in the FNP on the particle properties (size, PDI) and zeta potential by measuring with DLS. In general, the three polymers commonly produced P-NPs with the smallest size and the lowest PDI under turbulent jet flow condition at different polymer concentrations, compared to the flow regimes of laminar and V & T conditions, including bulk method (Fig. 3A–C, and Table 3). It obviously indicates that the faster mixing in the FNP facilitates rapid nucleation and homogeneous precipitation.[26] Moreover, the P-NPs prepared from P(St-MA) at a concentration of 7 mg mL^{-1} in a turbulent jet flow mode showed an average size of 141 nm, respectively, whereas the P-NPs obtained from P(MMA-MAA) under the same conditions were measured at 197 nm.

Table 3 The average size, PDI value, and zeta potential of P(St-MA) NPs at different Re numbers

Flow regimes	Laminar	Vortex and turbulence	Turbulent jet
Average size (nm)	255	164	141
PDI	0.1	<0.1	<0.1
Zeta potential (mV)	−35	−31	−27

This can be explained by the difference in Ra values upon FNP. As shown in Table 1, the difference in Ra values for P(St-MA) and P(St-AA) is 34.9 (2.0 in THF, 36.9 in water) and 34.7 (0.8 in THF, 35.5 in water), while P(MMA-MAA) is only 29.6 (4.0 in THF, 33.6 in water). It is generally known that the large difference in Ra values increase the degree of supersaturation and occurs precipitation quickly, producing small and monodisperse P-NPs.[27,28]

In addition to the size and distribution, the surface charge of amphiphilic P-NPs is a very important parameter in determining the dispersion stability and interaction with the external environment.[29] Both P(St-MA) and P(MMA-MAA) NPs with –COOH groups, and P(St-AA) NPs with –OH groups all exhibit negative surface charges, *i.e.* zeta potential, by deprotonation in water. Moreover, the zeta potentials are different, depending on the preparation conditions with different mixing efficiencies and the characteristics of polymers.

First, when investigating the effect of production methods on zeta potential of P(St-MA) NPs, the NPs prepared by batch process are more negative than the NPs by FNP (Fig. 3D). In particular, three types of polymers commonly show that the P-NPs precipitated in a laminar flow exhibits more negative zeta potential than the P-NPs prepared in a turbulent jet (Fig. 3D–F). In the turbulent jet regime, rapid mixing can cause violent and instant insolubilization, indicating that the entangled hydrophilic–hydrophobic parts of amphiphilic random copolymers are not sufficiently aligned in a short time of precipitation. On the other hand, the rapid mixing favorably generates smaller particles of uniform size. However, under laminar flow and bulk conditions with relatively low mixing behavior, the hydrophilic part is partially arranged outward in water, while the hydrophobic part is guided inward by the swollen THF solvent, which can gradually grow into large particles. This highlights the importance of mixing to maintain precise control over P-NP size, zeta potential, and uniformity.

Secondly, upon speculation on the effect of polymer characteristics, two rapidly precipitating P(St-MA) NPs and P(St-AA) NPs reveal considerably different zeta potentials: −35 to −27 mV (Fig. 3D), −26 to −16 mV (Fig. 3E), respectively,

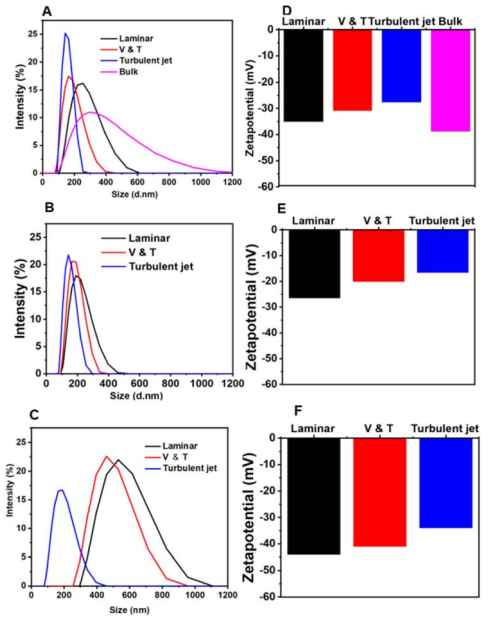

Fig. 3 Size distributions of nanoparticles obtained from (A) 7 mg mL^{-1} P(St-MA), (B) 3 mg mL^{-1} P(St-AA), (C) 7 mg mL^{-1} P(MMA-MAA) under various conditions. Zeta potentials of nanoparticles obtained from (D) 7 mg mL^{-1} P(St-MA), (E) 3 mg mL^{-1} P(St-AA), (F) 7 mg mL^{-1} P(MMA-MAA) by bulk or FNP.

© 2024 The Author(s). Published by the Royal Society of Chemistry

Open Access Article. Published on 14 June 2024. Downloaded on 12/27/2025 2:59:57 PM.
This article is licensed under a Creative Commons Attribution-NonCommercial 3.0 Unported Licence.

presumably due to different deprotonation tendency of –COOH and –OH groups. And the slowly precipitating P(MMA-MAA) NPs with –COOH groups exhibit relatively low zeta potential values in the range of −44 to −34 mV (Fig. 3F) due to better assembly as explained. With the results, P(St-MA) and P(MMA-MAA) NPs are considered to have better dispersion stability.[30]

To enhance the stability of the P-NPs, post-treatment aimed at lowering the zeta potential was performed. This process is explained in detail in Section 3.5 for more clarity.

3.4. Effect of polymer concentrations and co-solvent addition

As aforementioned, the turbulent jet regimes produced smaller size of P-NPs with narrow PDI using THF as a solvent and DI water as an anti-solvent. Actually, high polymer concentration generates large number of nuclei due to induced supersaturation, but as the viscosity increases, interchain entanglement and interactions also increase, which slows down diffusion movement and thus nucleation. Therefore, the size of P-NPs increases in proportion to concentration due to internuclear collisions and aggregate growth, as seen Fig. 4A. In addition, the larger the molecular weight of the polymer, the longer and heavier the chain, making it less soluble in the solvent, and the interaction between polymer chains increases, forming precipitated P-NPs similar to those at high concentrations. As the molecular weight of P(St-AA) is relatively low, the polymer chains dissolve well in the solvent, and entanglement and bonding between polymer chains decreases, resulting in excessive nucleation and smaller P-NP size.

Due to the constraints in further decreasing both mixing time and polymer concentration to reduce P-NP size, we have begun to consider the properties of solvent: solubility and diffusion. MeOH and EtOH are solvents that demonstrate higher diffusion coefficients for water compared to THF (Table S5 and S6†),[31–34] (Fig. S4A and B†). Fig. 4B and C show FNP experiments under turbulent jets by adding co-solvents EtOH and MeOH to 1 mg mL^{-1} P^{-1}(St-AA) polymer. When the co-solvent content is low range, the P-NP size gradually decreases, but as the additive content increases above a certain level, the P-NP size increases in a parabolic manner (Fig. 4B and C). The P-NPs prepared using THF as the sole solvent are 123 nm, but when 40% ethanol content is added, a noticeable decrease (37.5%) to minimum of 79 nm is observed. When 60% methanol content is added, a significant 45% reduction to minimum of 68 nm is shown. In other words, when added with a co-solvent that has better diffusion ability than THF, the P-NP size becomes smaller due to the effect of increasing supersaturation, and after a certain point, the polymer solubility decreases and the size of the P-NP increases, interpreting a competition phenomenon between diffusion and solubility.

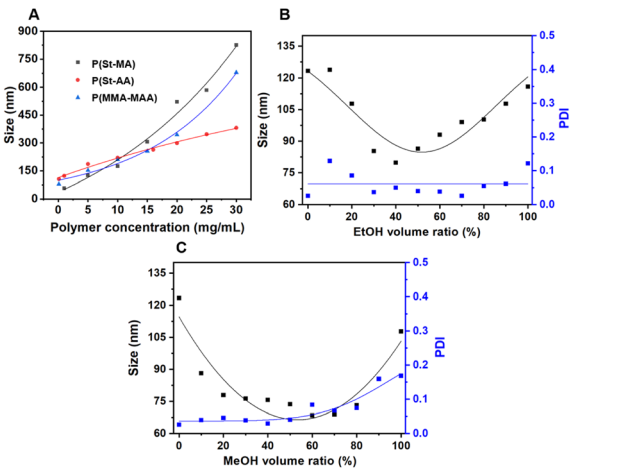

Fig. 4 Effect of (A) polymer concentration and co-solvents (B) EtOH and (C) MeOH addition into 1 mg mL^{-1} P(St-AA) on size/distribution of P-NPs under turbulent jet flow condition.

3.5. Effect of post-treatment in the solution

Inspired by the solvent annealing process of diblock copolymers, the post-treatment was conducted by gently placing the P-NPs in the mixed water-THF solution in the absence of co-solvent for 16 h. As a result, the evaporation of volatile THF may induce further self-assembly by slightly migrating hydrophilic parts onward the surface of P-NPs. As shown in Fig. 5, three types of P-NPs show a similar change in the zeta potentials by becoming more negative, as expected. The zeta potential of the P-NPs produced by the laminar gives the largest change in all cases, followed by the P-NPs obtained from V&T conditions, and the P-NPs prepared under turbulent jet flow showed less change. It is appeared that the P-NPs produced at low mixing laminar condition cause less entanglement of polymer chains, facilitating rearrangement of the hydrophilic parts, whereas the P-NPs from highly mixing turbulent jet flow has severe aggregation by interlocked chains, resulting in low rearrangement in the particle.

Comparing the P-NPs synthesized in laminar flow condition of Fig. 5A and C, the P(St-MA) NPs lowers the most significantly

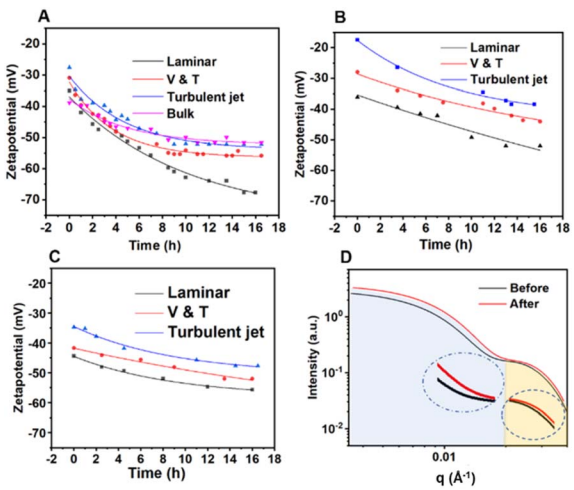

Fig. 5 Effect of post-treatment time on zeta potential of various nanoparticles from (A) P(St-MA), (B) P(St-AA), (C) P(MMA-MAA). (D) Change in shape factor fitting for P(St-MA) nanoparticles (50 nm initial) scattering contributions, before and after post-treatment, precipitated by water-THF solvent with no co-solvents.

Open Access Article. Published on 14 June 2024. Downloaded on 12/27/2025 2:59:57 PM. This article is licensed under a Creative Commons Attribution-NonCommercial 3.0 Unported Licence.

to −67 mV from initial −37 mV after post-treatment, while the P(MMA-MAA) NPs with identical –COOH groups show less change to negative zeta potential to −55 mV from −44 mV. This could be attributed to the lower pKa (1.9) of maleic acid, indicating strong deprotonation tendency in water. In contrast, methacrylic acid (pKa 4.7) are less acidic than maleic acid.[35–37] Note that high pKa (15.5) of allyl alcohol explain the smallest change to −51 mV from −36 mV in Fig. 5B.

In addition, the P(St-MA) NPs obtained the turbulent jet and the bulk conditions exhibit a similar change from −27 to −52 mV, from −38 to −51 mV, respectively, but for different reasons (Fig. 5A). The less rearrangement inside the P-NP may arise from strong interlocked chains in turbulent jet flow, aggregated and meshed chains in slow mixing of bulk condition that resulted in large size.

In an aqueous solution, amphipathic random copolymers give rise to P-NPs characterized by a core composed of hydrophobic segments and an outer shell consisting of hydrophilic copolymer brushes. The formation of this core-shell-like architecture is notably governed by the kinetic parameters governing self-assembly conditions. Therefore, we have incorporated small-angle X-ray scattering (SAXS) profile to assess structural alterations in P-NPs before and after post-treatment (Fig. 5D). The intensity profiles resembled core–shell form factors.[38–40] The shell thickness decreased from 10.25 nm to 9.70 nm, while the core size decreased from 8.46 nm to 8.30 nm, which is consistent with the shrinkage behavior of P-NPs during post-treatment as observed by DLS measurement. Notably, the size detected by SAXS is much smaller than the initial size (50 nm) and post-treated size (46 nm) by DLS that measured larger apparent sizes with Brownian motion of P-NPs (Fig. S5†).[41,42]

4 Conclusions

We present a straightforward and versatile coaxial micro-mixer designed for synthesizing a variety of P-NPs based on random amphiphilic copolymers in FNP. By characterizing the flow behaviors utilizing the micro-mixer, we successfully produced P(St-MA), P(St-AA), and P(MMA-MAA) NPs, allowing for particle size within the range of 51 to 819 nm by manipulating the polymer concentration and solvent system. Zeta potential detection further unveiled the exposure of hydrophilic functional groups on the P-NP surfaces when dispersed in water. Subsequent post-treatment further shows the effect on zeta potential of P-NPs. We believe this technology is a valuable addition to the field of nanotechnology based on random amphiphilic copolymers.

Author contributions

J. Joo, C. Park, and J. Yang designed the project and drafted the manuscript. H. Ahn measured SAXS. Jeong-Un leading the revision process. Dong-Pyo Kim conceived the project.

Conflicts of interest

There are no conflicts to declare.

Acknowledgements

We gratefully acknowledge the support from the National Research Foundation (NRF) of Korea grant funded by the Korean government (MSIP) (NRF-2017R1A3B1023598).

References

1 C. C. Shih, Y. C. Chiu, W. Y. Lee, J. Y. Chen and W. C. Chen, *Adv. Funct. Mater.*, 2015, **25**, 1511.
2 S. Y. Ong, C. Zhang, X. Dong and S. Q. Yao, *Angew. Chem., Int. Ed.*, 2021, **60**, 17797.
3 G. Fytianos, A. Rahdar and G. Z. Kyzas, *Nanomaterials*, 2020, **10**, 979.
4 X. Wu, Y. Qiao, H. Yang and J. Wang, *J. Colloid Interface Sci.*, 2010, **349**, 560.
5 C. A. Sanders, S. R. George, G. A. Deeter, J. D. Campbell, B. Reck and M. F. Cunningham, *Macromolecules*, 2019, **52**, 4510.
6 X. Zhu and M. Liu, *Langmuir*, 2011, **27**, 12844.
7 L. Li, K. Raghupathi, C. Song, P. Prasad and S. Thayumanavan, *Chem. Commun.*, 2014, **50**, 13417.
8 A. Honglawan, H. Ni, D. Weissman and S. Yang, *Polym. Chem.*, 2013, **4**, 3667.
9 X. Liu, J. S. Kim, J. Wu and A. Eisenberg, *Macromolecules*, 2005, **38**, 6749.
10 S. Imai, Y. Hirai, C. Nagao, M. Sawamoto and T. Terashima, *Macromolecules*, 2018, **51**, 398.
11 P. Guo, W. Guan, L. Liang and P. Yao, *J. Colloid Interface Sci.*, 2008, **323**, 229.
12 K. Balakrishnan and N. Murugasean, *Int. J. Nano Dimens.*, 2021, **12**, 76.
13 I. J. Joye and D. J. McClements, *Trends Food Sci. Technol.*, 2013, **34**, 109.
14 Y. Zeng, T. Xu, X. F. Hou, J. Liu, C. Chang and D. Chen, *ACS Appl. Polym. Mater.*, 2023, **5**, 3777.
15 L. N. Turino, B. Stella, F. Dosio, J. A. Luna and A. A. Barresi, *Drug Dev. Ind. Pharm.*, 2018, **44**, 934.
16 J. Tao, S. F. Chow and Y. Zhang, *Acta Pharm. Sin. B*, 2019, **9**, 4.
17 J. C. Cheng, PhD thesis, Iowa State University, 2010.
18 (*a*) H. Han, J. H. Yoon, G. R. Yi, W. I. Choi and J. M. Lim, *J. Ind. Eng. Chem.*, 2021, **97**, 411; (*b*) L. Jiang and S. Yao, *IEEE Trans. Nanotechnol.*, 2016, **15**, 828.
19 C. M. Hansen, Applications-Coatings and Other Filled Polymer Systems, *Hansen Solubility Parameters: A User's Handbook*, CRC Press:Boca Raton, FL, USA, 2007, 2nd edn.
20 B. Sanchez-Lengeling, L. M. Roch, J. D. Perea, S. Langner, C. J. Brabec and A. Aspuru-Guzik, *Adv. Theory Simul.*, 2019, **2**, 1800069.
21 J. M. Lim, A. Swami, L. M. Gilson, S. Chopra, S. Choi, J. Wu and O. C. Farokhzad, *ACS Nano*, 2014, **8**, 6056.
22 C. Sinturel, M. Vayer, M. Morris and M. A. Hillmyer, *Macromolecules*, 2013, **46**, 5399.
23 C. Cummins, R. A. Kelly, A. Gangnaik, Y. M. Georgiev, N. Petkov, J. D. Holmes and M. A. Morris, *Macromol. Rapid Commun.*, 2015, **36**, 762.

© 2024 The Author(s). Published by the Royal Society of Chemistry

Open Access Article. Published on 14 June 2024. Downloaded on 12/27/2025 2:59:57 PM.
This article is licensed under a Creative Commons Attribution-NonCommercial 3.0 Unported Licence.

24 (*a*) S. Gimondi, H. Ferreira, R. L. Reis and N. M. Neves, *ACS Nano*, 2023, **17**, 14205; (*b*) Y. Liu, G. Yang, Y. Hui, S. Ranaweera and C. X. Zhao, *Small*, 2022, **18**, 2106580.
25 N. T. Thanh, N. Maclean and S. Mahiddine, *Chem. Rev.*, 2014, **114**, 7610.
26 (*a*) M. Kakran, N. G. Sahoo, I. L. Tan and L. Li, *J. Nanopart. Res.*, 2012, **14**, 1; (*b*) T. Maki, S. Takeda, Y. Muranaka and K. Mae, *Front. Chem. Eng.*, 2021, **3**, 742322.
27 Y. Liu, G. Yang, D. Zou, Y. Hui, K. Nigam, A. P. Middelberg and C. X. Zhao, *Ind. Eng. Chem. Res.*, 2019, **59**, 4134.
28 T. J. Neal, A. J. Parnell, S. M. King, D. L. Beattie, M. W. Murray, N. S. Williams and O. O. Mykhaylyk, *Macromolecules*, 2018, **51**, 1474.
29 M. Shah, M. I. Naseer, M. H. Choi, M. O. Kim and S. C. Yoon, *Int. J. Pharm.*, 2010, **400**, 165.
30 M. Arulprakasajothi, K. Elangovan, U. Chandrasekhar and S. Suresh, *Therm. Sci.*, 2018, **22**, 477.
31 Z. J. Derlacki, A. J. Easteal, A. V. J. Edge, L. A. Woolf and Z. Roksandic, *J. Phys. Chem.*, 1985, **89**, 5318.
32 S. Y. Noskov, G. Lamoureux and B. Roux, *J. Phys. Chem. B*, 2005, **109**, 6705.
33 T. Seydel, R. M. Edkins and K. Edkins, *Phys. Chem. Chem. Phys.*, 2019, **21**, 9547.
34 M. N. Rodnikova, Z. S. Idiyatullin, I. A. Solonina and D. A. Sirotkin, *Russ. J. Phys. Chem. A*, 2019, **93**, 275.
35 R. Mlih, J. Suazo-Hernández, Y. Liang, E. Tombácz, R. Bol and E. Klumpp, *Colloids Interfaces*, 2023, **7**, 5.
36 H. Morinaga, F. Tsuneishi, S. Taniguchi and G. Kawakami, *Tetrahedron Lett.*, 2014, **55**, 3768.
37 A. Wong, F. M. De Oliveira, C. R. T. Tarley and M. D. P. T. Sotomayor, *React. Funct. Polym.*, 2016, **100**, 26.
38 M. Hildebrandt, S. Lazarev, J. Pérez, I. A. Vartanyants, J. M. Meijer and M. Karg, *Macromolecules*, 2022, **55**, 2959.
39 D. Lombardo, P. Calandra and M. A. Kiselev, *Molecules*, 2020, **25**, 5624.
40 S. L. Gawali, K. C. Barick, V. K. Aswal, M. Basu and P. A. Hassan, *J. Phys. Chem. B*, 2020, **124**, 3418.
41 C. J. Kim, K. Sondergeld, M. Mazurowski, M. Gallei, M. Rehahn, T. Spehr and B. Stühn, *Colloid Polym. Sci.*, 2013, **291**, 2087.
42 S. Pabisch, B. Feichtenschlager, G. Kickelbick and H. Peterlik, *Chem. Phys. Lett.*, 2012, **521**, 91.

© 2024 The Author(s). Published by the Royal Society of Chemistry